Title

Transport of Neutral and Charged Solutes in Imidazolium-Functionalized Poly(phenylene oxide) Membranes for Artificial Photosynthesis

Journal

Industrial & Engineering Chemistry Research, 59(12)

ISSN

0888-5885

Authors

Dischinger, Sarah M
Gupta, Shubham
Carter, Blaine M
et al.

Publication Date

2020-03-25

DOI

10.1021/acs.iecr.9b05628

Peer reviewed

Transport of neutral and charged solutes in imidazolium-functionalized poly(phenylene oxide) membranes for artificial photosynthesis

*Sarah M. Dischinger, Shubham Gupta, Blaine M. Carter, and Daniel J. Miller**

Joint Center for Artificial Photosynthesis, Lawrence Berkeley National Laboratory, Berkeley, CA, 94720

**danieljmiller@lbl.gov, +1 (510) 495-2353*

Abstract

Anion exchange membranes (AEMs) play an essential role in artificial photosynthesis devices, which photoelectrochemically convert CO_2 and water into useful products. AEMs allow the transport of charge carriers between electrodes while minimizing the transport of CO_2 reduction products (*e.g.*, ethanol). Fundamental transport studies in AEMs relevant to artificial photosynthesis are uncommon. Herein, we describe the preparation of an imidazolium-functionalized poly(phenylene oxide) membrane. Membrane transport properties were controlled by systematic variation of the degree of imidazolium functionalization, which induced changes in the membrane water volume fraction. Ethanol permeability and ionic conductivity increased with membrane water volume fraction. Consequently, membranes of relatively high ionic conductivity exhibited relatively high ethanol permeability, presenting a tradeoff in the transport properties desirable for artificial photosynthesis applications. This work seeks to enable optimization of AEMs for artificial photosynthesis through systematic study of membrane structure (water volume fraction) and its relevance to alcohol transport and electrolyte ion conductivity.

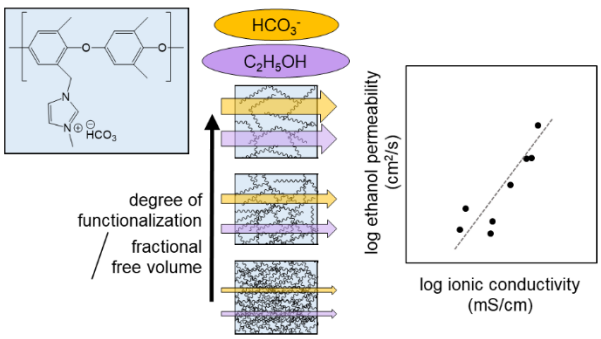

1. Introduction

The (photo)electrochemical conversion of CO_2 using solar energy (*i.e.*, artificial photosynthesis) is of growing interest as a means to produce valuable products, such as non-petroleum based liquid fuels and chemical feedstocks.[1–4] Artificial photosynthesis devices typically consist of an anode and a cathode separated by an ion exchange membrane and liquid electrolyte.[5–8] As CO_2 (introduced as a humidified gas or dissolved in the liquid electrolyte) is reduced to gaseous or liquid products at the cathode, water is oxidized to oxygen at the anode.[5,6] Near-neutral or alkaline electrolyte conditions usually favor CO_2 reduction (CO_2R) to C_{2+} products over the competing hydrogen evolution reaction.[6,9–11] The electrolyte charge carrier between the anode and cathode in the liquid electrolyte is commonly bicarbonate or carbonate, although supplemental electrolyte charge carriers are sometimes employed.[7,9,12–14] Given that the primary electrolyte charge carriers are anions, anion exchange membranes (AEMs) are often employed in artificial photosynthesis devices because they more readily promote anion transport between the electrodes than cation exchange membranes.[6,15] High charge carrier transport fluxes support high device current densities and reduce polarization losses.[6,16]

While the range of potential CO_2R products is large, products of specific interest are alcohol fuels (*e.g.*, methanol and ethanol) due to their high energy density and market value

relative to energy input.[3,5,17] Crossover of products from the cathode to the anode lowers overall device efficiency because these reduced species may undergo oxidation at the anode, which leads to product loss and wasted energy.[18–21] Therefore, a membrane that transports carbonate/bicarbonate ions while minimizing the transport of small product alcohols is expected to enable high efficiency artificial photosynthesis devices.[6,16,21] Achieving highly selective transport (*i.e.,* high rates of electrolyte ion transport and low rates of product alcohol transport) is challenging because increasing the transport of an electrolyte charge carrier is often correlated with increased transport of other species through the membrane.[22] For example, an increase in conductivity within a series of AEMs correlated with an increase in co-ion transport, decreasing the permselectivity of the membrane.[23] This phenomenon is encountered in gas separation, desalination, and other membrane separations, and is commonly referred to as the selectivity/permeability tradeoff.[23–25] Relatively few studies have explicitly investigated the selectivity/permeability trade-off as it pertains to artificial photosynthesis device performance; however, such studies would contribute to the development of devices that are commercially viable.[14,22]

Despite widespread usage, commercial availability, and multiple reviews of AEMs, a comprehensive understanding of how AEM structure correlates with transport phenomena has not been realized.[19,20,26–31] While the market availability of these materials has made them popular in (photo)electrochemical CO_2R studies, the proprietary nature of these materials makes it difficult to ascertain a detailed understanding of how membrane chemistry and structure affect device performance *vis-à-vis* water, electrolyte ion, and CO_2R product transport.[6,17,32] By employing a material platform with chemical and/or structural parameters that can be tuned in a systematic fashion, it may be possible to begin understanding how membrane composition

affects the efficiency and productivity of artificial photosynthesis devices. This understanding could enable synthesis of membranes tailor-made for this purpose or improved decision making when choosing from commercially available materials. While several studies have correlated salt transport to AEM structural and chemical properties, few studies have explored uncharged solute (*e.g.*, alcohol) transport through AEMs.[22,23,31,33–37] More studies are needed to understand the complexity of transport through diverse membrane materials in a range of applications, including artificial photosynthesis.[4,14]

Imidazolium-functionalized poly(phenylene oxide)-based membranes offer a platform that enables explicit study of membrane structure and transport properties within the context of artificial photosynthesis. Poly(phenylene oxide) (PPO)-based AEMs are of interest for artificial photosynthesis devices because, in other applications, they have demonstrated high conductivity and relatively robust alkaline stability.[20,38–40] PPO is also advantageous because it is relatively inexpensive, commercially available, and can be easily functionalized with a variety of chemical moieties.[23,40–44] Functionalization of the PPO with cationic imidazolium or quaternary ammonium groups converts this neutral polymer into an anion exchange material; imidazolium and quaternary ammonium functional groups have demonstrated relatively high conductivities and stability in alkaline conditions, offering potential for use in artificial photosynthesis devices.[42,45–47] The work presented here focuses on imidazolium-functionalized PPO. While the studies referenced above investigated the role of various structural attributes of the polymer on membrane conductivity and alkaline stability, only one considered small uncharged solute transport.[43] However, the conflicting transport goals of the AEM in artificial photosynthesis devices (*i.e.*, high electrolyte ion conductivity and low CO_2R product permeability) require an understanding of the correlation between charged and uncharged solute transport in these

materials. Therefore, further studies on imidazolium-functionalized PPO materials would contribute to optimization of AEMs for artificial photosynthesis devices.

This work aims to advance the understanding of charged and uncharged solute transport through AEMs by examination of structure-transport relationships relevant to artificial photosynthesis devices *via* an un-crosslinked imidazolium-functionalized PPO material platform. The chemical structure of the imidazolium-functionalized PPO was modified by varying the degree of functionalization (*i.e.*, ion exchange capacity). Localizing this work within the context of artificial photosynthesis, the conductivity of bicarbonate (a primary charge carrier in CO_2R) and the permeability of ethanol (a target CO_2R product) were studied with respect to polymer functionalization.[5,6] As rates of solute transport appear to be strongly linked to AEM water uptake, [22,23] the transport of bicarbonate and ethanol was also correlated with the structural parameter of membrane water volume fraction. While the counterion of interest for artificial photosynthesis devices is bicarbonate, it is informative to consider the properties of membranes in the bromide form because, as will be shown below, the variation of counterion results in a difference of water uptake without changing the ion exchange capacity of the material. Therefore, by comparing the performance of membranes in both the bicarbonate and bromide forms, it is possible to consider the structure (*i.e.*, water volume fraction) of the membrane apart from its ion exchange capacity, so as to elucidate the impact of these factors on membrane performance. To contextualize these results, the transport properties of the imidazolium-functionalized PPO membrane were compared with the commercial AEM Selemion AMV.

2. Experimental

2.1 Materials

Poly(2,6-dimethyl-phenylene oxide), diethyl ether, and methanol (99%) were purchased from Sigma Aldrich and used as received. *N*-bromosuccinimide (NBS) and potassium bicarbonate (99%) were purchased from Alfa Aesar and used as received. Azobisisobutyronitrile (AIBN) (Matrix Scientific, 97%), chlorobenzene (Millipore, 99%), 1-methyl-2-pyrrolidone (NMP, JT Baker, 99%), 1-methylimidazolium (TCI, 99%), and ethanol (Koptec, 99%) were used as received. Deionized (DI) water was supplied by an EMD Millipore Milli-Q Integral 3 water purification system (18.2 MΩ cm at 25 °C, 1.2 ppb TOC). Selemion AMV (AGC Engineering Co., Ltd.) was stored in DI water until use.

2.2 Membrane Preparation

An example synthesis of brominated PPO is as follows. Poly(2,6-dimethyl-phenylene oxide) (10 g), dry NBS (9.9 g), and AIBN (0.4 g) were dissolved in chlorobenzene (200 mL) in a 500 mL round-bottom flask with a stir bar and reflux condenser. The reaction temperature was maintained at 135 ºC for at least 4 h. The brominated PPO was recovered *via* precipitation in methanol and dried under vacuum (<1 Torr, 40 ºC). ^{1}H NMR (Bruker Ascend^{TM} 500) was used to confirm the purity of the product (see Figure S1 in the Supplemental Information). The number of brominated methyl groups was adjusted by varying the amount of NBS added.

Imidazolium-functionalized PPO (ImPPO) was synthesized as follows. Brominated PPO (3.1 g) was dissolved in NMP (23 mL) with 1-methylimidazolium (1.3 g) in a 100 mL round-bottom flask with a stir bar and reflux condenser. The reaction temperature was maintained at 80 ºC for at least 12 h. ImPPO was precipitated in diethyl ether and then dried under vacuum (<1

Torr, 40 ºC). Enough 1-methylimidazolium was added to convert all pendant bromine to imidazolium; this conversion was evaluated by ^{1}H NMR (see Figure S2 in the Supplemental Information). ^{1}H NMR was also used to evaluate the purity of each compound and the degree of functionalization χ (*i.e.*, the percent of methyl pendants with an imidazolium attached) (see calculations in the Supplemental Information). The ion exchange capacity (IEC) (*i.e.*, the concentration of imidazolium moieties in the dry polymer) was calculated from the degree of functionalization of the polymer, as shown in the Supplemental Information. Multiple publications on PPO-based AEMs have calculated IEC values from ^{1}H NMR spectra that are within 10% of the values determined *via* a titration method, another common technique for IEC determination.[45,48–50]

Membranes were fabricated by dissolving ImPPO-χ (0.3 g) in NMP (~5.5. g) at room temperature. The solution was filtered through a 1-µm PTFE filter (Thermo Scientific) into a Teflon dish 6 cm in diameter that was pre-wetted with methanol. The membranes were dried at 80 ºC for about 2.5 days. Membranes were stored sealed until use.

The bromide counterion in the ImPPO-χ membranes was exchanged to bicarbonate by soaking ImPPO-χ membranes in aqueous 1 M potassium bicarbonate solution for 48 h, replacing the exchange solution three times. During this process, the pH was monitored to ensure that no significant shift in carbonate speciation had occurred. The pH was found to vary from 8.3 to 9.0. Even at the highest pH measured, the concentration of bicarbonate was still an order of magnitude greater than the concentration of carbonate.[51] Subsequently, the membrane was soaked in DI water for at least 24 h, or until the membranes reached a constant hydrated weight. The water was replaced at least once during DI soaking. Samples were stored in DI water until further use. The complete reaction scheme, including ion exchange, is presented in Figure 1.

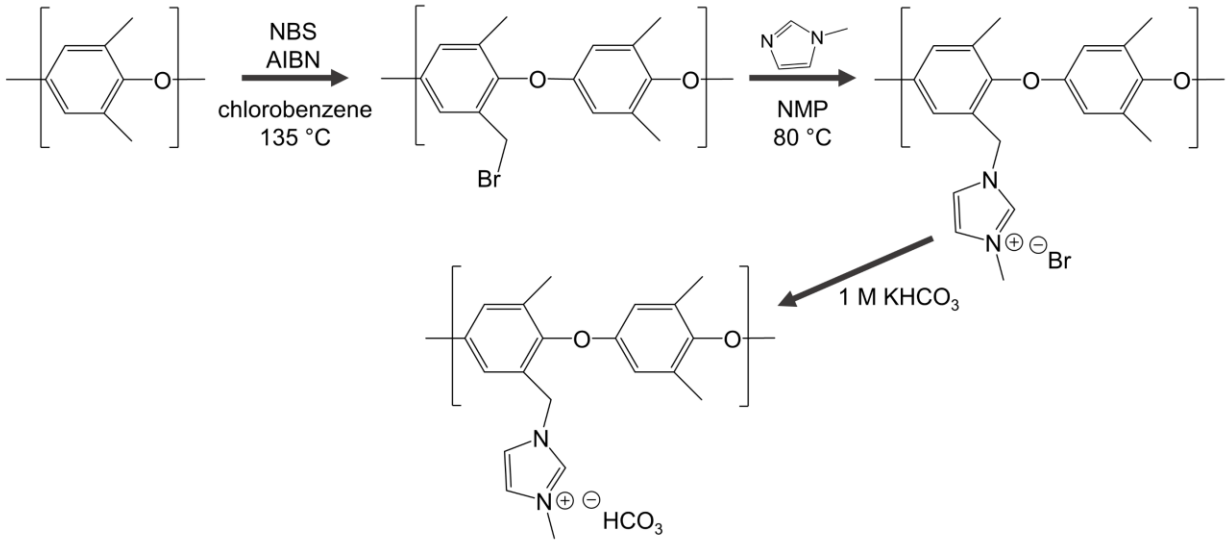

Figure 1. Synthetic route and final structure of ImPPO-χ, where χ is the percent methyl groups functionalized. One or both of the methyl groups on any aromatic ring may be functionalized.

For water uptake and density measurements, membranes were dried under vacuum (<1 Torr, 40 ºC) until a constant dry weight was achieved. Completeness of ion exchange was evaluated by elemental analysis of the dry membrane cross section using energy dispersive spectroscopy (Bruker Quanteax 200 EDS) paired with scanning electron microscopy (SEM FEI Quanta 250 FEG). The commercial Selemion AMV anion exchange membrane was exchanged to bicarbonate and using the same procedure. Selemion AMV was exchanged to bromide using the same procedure except that the anion exchange solution was an aqueous 1 M sodium bromide solution.[22]

For the following characterizations, at least three individually-prepared membranes were evaluated, and the errors presented in each figure represent one standard deviation, calculated *via* error propagation analysis.[52]

2.3 Water Uptake

Membranes were soaked in DI water until they reached a constant weight (at least 48 h). Hydrated membranes were blotted with a Kimwipe before each weight measurement to remove liquid on the surface and returned to DI water between measurements to ensure that the membranes were always fully hydrated. Once the hydrated weight was measured, the membranes were dried under vacuum (< 1 Torr, 40 ºC) until they reached a constant weight (at least 48 h). When a constant dry weight was measured, the thickness and diameter of each sample were also measured in order to calculate the density of the dry membrane.

Water uptake, *w*, was calculated as follows:[23]

$$w = \frac{m_h - m_d}{m_d} \qquad \text{Equation 1}$$

where m_h is the mass of the water-swollen membrane and m_d is the mass of the dry membrane. Assuming volume additivity, which has been shown to be reasonable for several charged polymer systems, water volume fraction (ϕ_w) was calculated as follows: [23,53]

$$\phi_w = \frac{w}{w + \frac{\rho_w}{\rho_p}} \qquad \text{Equation 2}$$

where ρ_w is the density of water (1 g/cm^3) and ρ_p is the density of the dry membrane. While the ion exchange capacity (IEC) is the concentration of imidazolium groups in the dry polymer, the IEC does not necessarily accurately represent the concentration of charged moieties in the water-swollen membrane. The fixed charge density, *i.e.*, the concentration of imidazolium groups, C_i, in the water-swollen membrane, was calculated as follows: [23]

$$C_i = \frac{IEC}{\frac{w}{\rho_w} + \frac{1}{\rho_p}}$$ Equation 3

2.4 Ethanol Permeability

Ethanol permeability in the water-swollen membranes was measured using a standard diffusion cell (Adams and Chittenden Scientific Glassware, Berkeley CA). An *in situ* ATR-FTIR probe (Mettler-Toledo ReactIR 15 with a shallow tip 9.5 mm DSun AgX DiComp probe) was used to detect the evolving ethanol concentration in the receiver cell (initially containing DI water). The diffusion cell halves were jacketed and a recirculating water bath was used to maintain the temperature of the diffusion cell at (25.0 ± 0.7) ºC. The initial donor cell concentration was 1 M ethanol in DI water. Permeability was calculated by fitting the time-resolved concentration data in the receiver cell to the Yasuda model.[36] The details of this experimental apparatus and associated methods have been previously published and are included in the Supplemental Information.[36,54]

2.5 Ionic Conductivity

In-plane conductivity of the water-swollen membranes was measured by potentiostatic electrochemical impedance spectroscopy using a four-point conductivity cell (BekkTech BT-110). The cell was submerged in DI water at room temperature. A Biologic VSP-300 potentiostat was used to vary the AC voltage about the open circuit potential at an amplitude of 80 mV. Measurements were collected over a frequency range of 0.5 MHz to 0.1 Hz. The membrane resistance (*R*) was taken as the impedance intercept with the real axis on a Nyquist plot.[42,55] (See

Supplemental Information for more detail.) Membrane conductivity (κ) was calculated from resistance as follows:[56–58]

$$\kappa = \frac{l}{Rz\delta} \quad \text{Equation 4}$$

where l is the length between the sensing probes, z is the width of the sample, and δ is the thickness of the sample.

3. Results and Discussion

3.1 Physical characterization of the membrane

PPO was functionalized with 1-methylimidazolium to three degrees of functionalization. The maximum degree of functionalization was limited to 24 % because membranes at higher degrees of functionalization dissolved in water during water uptake experiments. Analysis by ^{1}H NMR confirmed that functionalization occurred only at the benzyl position, rather than at the aryl position.[44] ^{1}H NMR analysis also confirmed that, for all degrees of functionalization, the conversion of brominated PPO to ImPPO was greater than 95 %. Figure 1 presents the structure of the family of ImPPO-χ materials prepared. The degree of functionalization, χ, (*i.e.*, the percent of methyl pendants that had imidazolium moieties) was calculated from the ^{1}H NMR spectra as the ratio of peak areas associated with the methylene hydrogens (around 5.3 ppm) and the methyl hydrogens (around 2.0 ppm) (see calculation in the Supplemental Information).[59] One or both of the methyl pendants on any aromatic ring may be functionalized with imidazolium; χ is the percent methyl groups functionalized (rather than the percent aromatic rings functionalized).

The speciation of carbonate in the anion exchange soak solution was monitored by pH; in all cases, the concentration of bicarbonate was at least an order of magnitude greater than that of carbonate, suggesting that bicarbonate was the majority counterion in the AEMs.[6,51] Elemental

analysis *via* energy dispersive spectroscopy of the cross section of the exchanged ImPPO-χ membranes detected insignificant signal associated with the presence of bromide, demonstrating that the exchange of the bromide anion for bicarbonate anion was nearly complete. It should be noted, however, that when Selemion AMV was subjected to the same ion exchange procedure, an incomplete exchange of anions was observed (see Figure S3 in the Supplemental Information), suggesting that some chloride remained in the membrane even after exchange. It is unlikely that changing the soak conditions would achieve complete exchange in the Selemion membranes, since these membranes were already soaked in the exchange solution for over 48 hours and the exchange solution was changed at least three times during the soak. Therefore, these membranes were used after being subjected to the same anion exchange procedure as the ImPPO membranes.

Table 1 provides some of the physical properties of the ImPPO-χ materials in the bicarbonate form as well as those of commercial Selemion AMV. While the Selemion AMV membrane is reinforced by a PVC mesh, other studies have concluded that any effect of such reinforcement on the material transport properties is small.[31] Therefore, the effects of the mesh were not considered separately, and the properties of Selemion that are discussed herein are properties of the composite membrane, as have been reported elsewhere.[60] To provide context for the values presented in Table 1, the typical range of IEC in ion exchange membranes is 0.1 – 2.7 meq./g while the typical range of water uptake is 9 – 180%.[19,27,31,42]

Table 1. Series of ImPPO-χ materials and commercial Selemion AMV. All properties are given for membranes in the bicarbonate form. χ was determined by ^{1}H NMR. IEC was calculated based on χ. Density was calculated from geometric measurements.

Polymer ID	χ (%)	IEC (mmol/g dry polymer)	Dry Membrane Density (g/cm^3)	Dry Membrane Thickness (μm)	Water Uptake (%)
ImPPO-11	11	1.4	1.0 ± 0.1	100 ± 20	19 ± 3
ImPPO-19	19	2.1	1.1 ± 0.1	130 ± 10	61 ± 4
ImPPO-24	24	2.4	1.0 ± 0.1	130 ± 20	209 ± 9
Selemion AMV		1.85 [30]	1.13 ± 0.04	104 ± 2	15 ± 2

3.2 Transport in ImPPO-χ membranes

3.2.1 Water uptake

Solute permeability in water-swollen polymers can be described within the framework of free volume theory as described by the Yasuda model, where the free volume is the space available for solute transport between polymer chains.[28,61–63] An important assumption of this model is that, in a hydrated membrane, water fills all of the available free volume elements, and that the degree of hydration is strongly correlated with the free volume.[28,61–63] Specifically, all else being equal in the polymer, the size of the free volume regions increases with degree of hydration of charged polymers, thereby increasing the solute's mobility.[35,63] Charged polymers often swell (*i.e.*, increase in degree of hydration) significantly in aqueous environments because the ionic groups attached to the polymer backbone are highly solvated by water.[28] Therefore, understanding solute transport in the charged ImPPO-χ materials begins with understanding their water uptake.

The degree of functionalization and the counterion influenced the water uptake of ImPPO-χ membranes (Figure 2a). Water uptake increased with increasing degree of

functionalization. This result can be explained by the solvation of greater numbers of charged moieties present in more highly-functionalized materials, and corroborates results reported for other ion exchange materials.[22,23,33,37] Additionally, membranes in the bicarbonate form generally sorbed more water than those of the same degree of functionalization in the bromide form, showing similar results to those reported elsewhere.[64] One factor that may contribute to this difference in water sorption is the difference in hydration number between the counterions: bromide typically has a hydration shell of six water molecules, while bicarbonate has a hydration shell of seven or eight water molecules.[64–66]

While water uptake itself does not provide direct information about the number or size of free volume elements within the membrane, it does permit calculation of the membrane water volume fraction, which correlates with the free volume available for solute transport.[63] Following the trend in water uptake, membranes with a higher degree of functionalization had a higher water volume fraction (Figure 2b). Due to the greater degree of water uptake by membranes in the bicarbonate form than those in the bromide form, membranes in the bicarbonate form also had a greater water volume fraction. The structure of the ImPPO-χ membrane (specifically, the free volume available for solute transport) varied with the degree of functionalization and the counterion associated with imidazolium. By considering bromide as a counterion in this study, it was possible to vary the water volume fraction of the material without changing the material's degree of functionalization. Therefore, though bromide counterions would likely not be encountered in artificial photosynthesis devices, it enabled an additional way to vary the structural properties and observe the impact of those structural changes on transport through the membrane.

ImPPO-χ membranes of higher degrees of functionalization had higher concentrations of charge in the dry polymer, but due to concurrent increases in water uptake, did not always have higher charge density of the swollen membrane *(i.e.*, fixed charge density). The fixed charge density influences the concentration of mobile charge carriers in the membrane and, therefore, the conductivity.[23,35] For the bromide form ImPPO-χ materials, an increase in degree of functionalization resulted in a moderate increase in fixed charge density when the degree of functionalization was increased from 11 to 19 %, and no change in fixed charge density when the degree of functionalization was increased further to 24 % (Figure 2c). For membranes in the bicarbonate form, the fixed charge density did not increase with an increase in the degree of functionalization from 11 to 19 %, and decreased as the degree of functionalization was further increased to 24 %. This decrease in fixed charge density can be attributed to a very high degree of water uptake (*cf*., Figure 2a and Equation 3) at the highest degree of functionalization. Similar trends of decreasing fixed charge density with increasing degree of functionalization have been observed in other polymer families.[33]

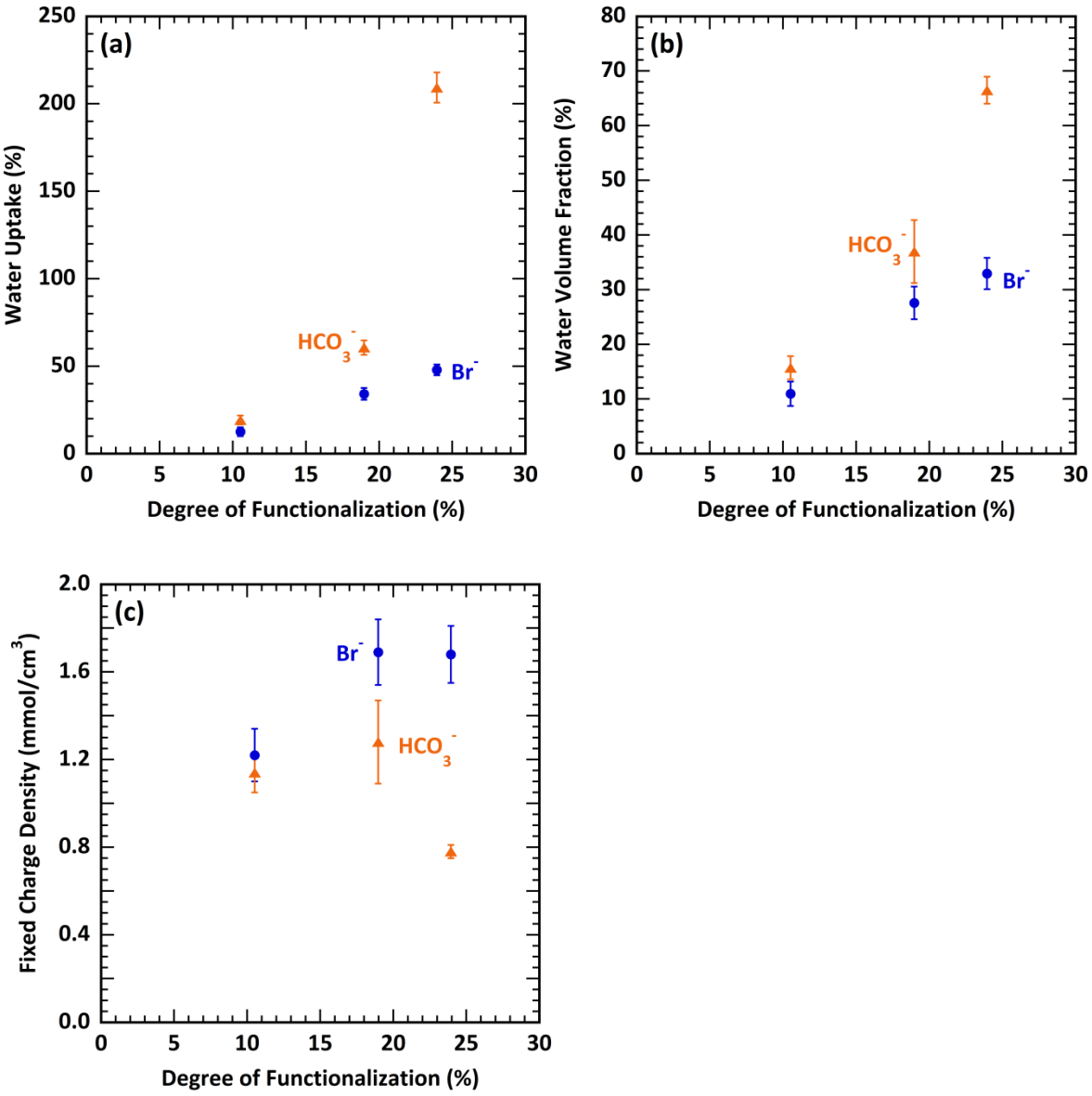

Figure 2. Water uptake (a), water volume fraction (b), and fixed charge density (c) as a function of degree of functionalization, χ, for ImPPO-χ materials in Br^- (blue circles) and HCO_3^- (orange triangles) forms.

3.2.2 Ethanol permeation

One of the primary functions of the membrane in artificial photosynthesis devices is to prevent product migration between the electrodes.[6] Ethanol is one aqueous CO_2R product of

interest, and its migration to the anode can potentially compromise device efficiency due to re-oxidation to CO_2 and product loss.[5,6,13,16,21] Therefore, membranes with low ethanol permeability are likely advantageous for artificial photosynthesis devices. Within the family of ImPPO-χ materials, membranes with high degrees of functionalization exhibited higher ethanol permeabilities than membranes with lower degrees of functionalization (Figure 3). Additionally, membranes in the bicarbonate form exhibited higher ethanol permeabilities than membranes of the same degree of functionalization in the bromide form.

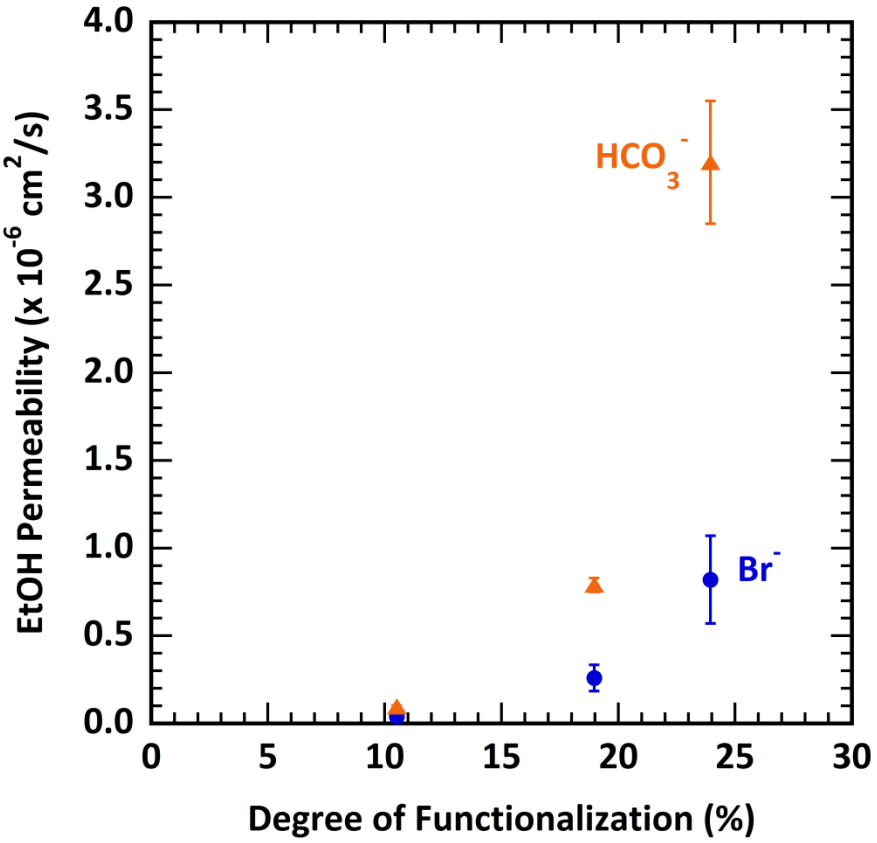

Figure 3. Ethanol permeability as a function of degree of functionalization, χ, for ImPPO-χ materials in Br^- (blue circles) and HCO_3^- (orange triangles) forms.

As mentioned above, ethanol moves through the membrane *via* available free volume elements as proposed by Yasuda *et al.*[61,62] The average diffusion coefficient of a solute *i* in a hydrated membrane is related to the inverse of the membrane water volume fraction (ϕ_w) as follows:

$$\bar{D}_i = D_{0,i} exp\left[-B\left(\frac{1}{\phi_w} - 1\right)\right] \qquad \text{Equation 5}$$

where $D_{0,i}$ is the diffusion coefficient of solute *i* in pure water and *B* is an empirical constant.[61] The diffusion of a solute in the hydrated membrane is linked to its permeability through the solution-diffusion model, which describes the permeability of a solute in a dense (*i.e.*, non-porous) membrane as the product of its diffusivity and solubility in the membrane.[67] The exponential relationship between permeability and inverse water volume fraction shown in Figure 4 suggests that available free volume principally governs ethanol transport in this family of ImPPO-χ materials. Such a relationship has been observed for small solutes (*e.g.*, simple salts and small organic molecules) in other dilute or semi-dilute (*i.e.*, highly hydrated) charged polymers.[22,37,68] To provide a point of comparison with a commercial membrane frequently employed in artificial photosynthesis devices, Selemion AMV is included in Figure 4. Selemion AMV, in both the bicarbonate and bromide forms, exhibited a relatively low ethanol permeability that was comparable to an ImPPO-χ material with a similarly low water volume fraction. No strong correlation was observed between ethanol permeability and fixed charge concentration (Figure S6 in Supplemental Information), which is unsurprising because the transport of uncharged solutes has been shown to be largely unaffected by the presence of fixed charged groups in studies of charged and uncharged membranes.[37] Within the family of ImPPO-χ materials studied herein, the water uptake varied with fixed charge concentration. To more

explicitly study the impact of fixed charge concentration on ethanol permeability, materials of varied fixed charge concentration with similar water uptakes should be studied.

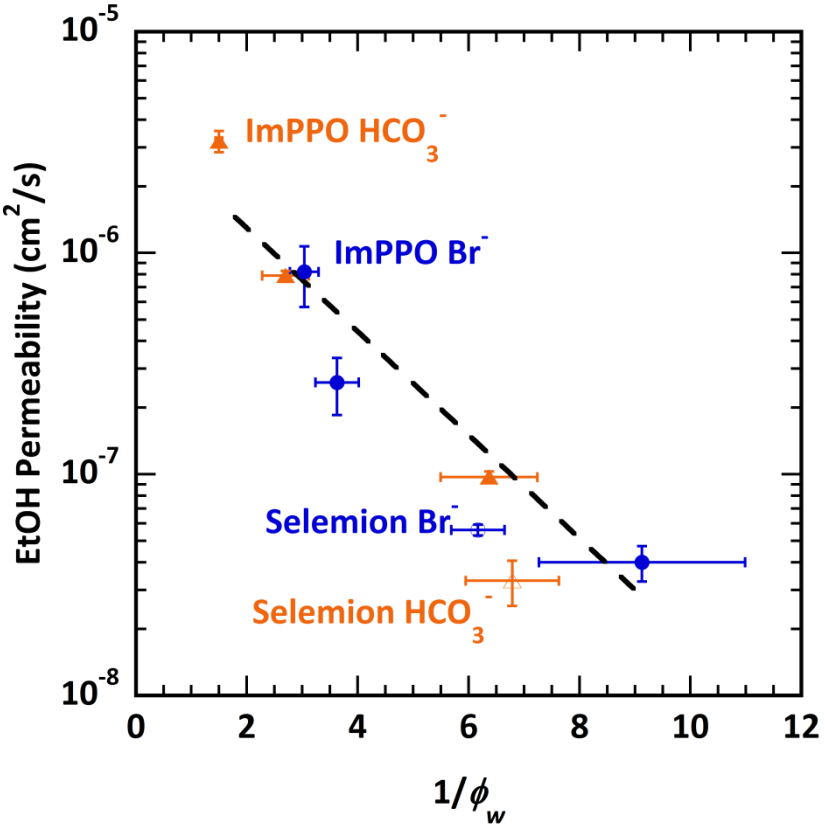

Figure 4. Ethanol permeability as a function of inverse water volume fraction for ImPPO-χ (filled symbols) and Selemion AMV (empty symbols) membranes in Br^- (blue circles) and HCO_3^- (orange triangles) forms. The line is a regression on the ImPPO-χ membrane data.

3.2.3 Ion Conductivity

The bicarbonate anion is the dominant charge-carrying electrolyte species in many recently reported CO_2R devices, and its transport across the membrane is essential to maintain device operation.[6,32] Within the family of ImPPO-χ materials, membranes with high degrees of functionalization exhibited higher conductivities than those with low degrees of functionalization

(Figure 5). Furthermore, membranes in the bromide form exhibited lower conductivities than membranes of the same degree of functionalization in the bicarbonate form (Figure 5).

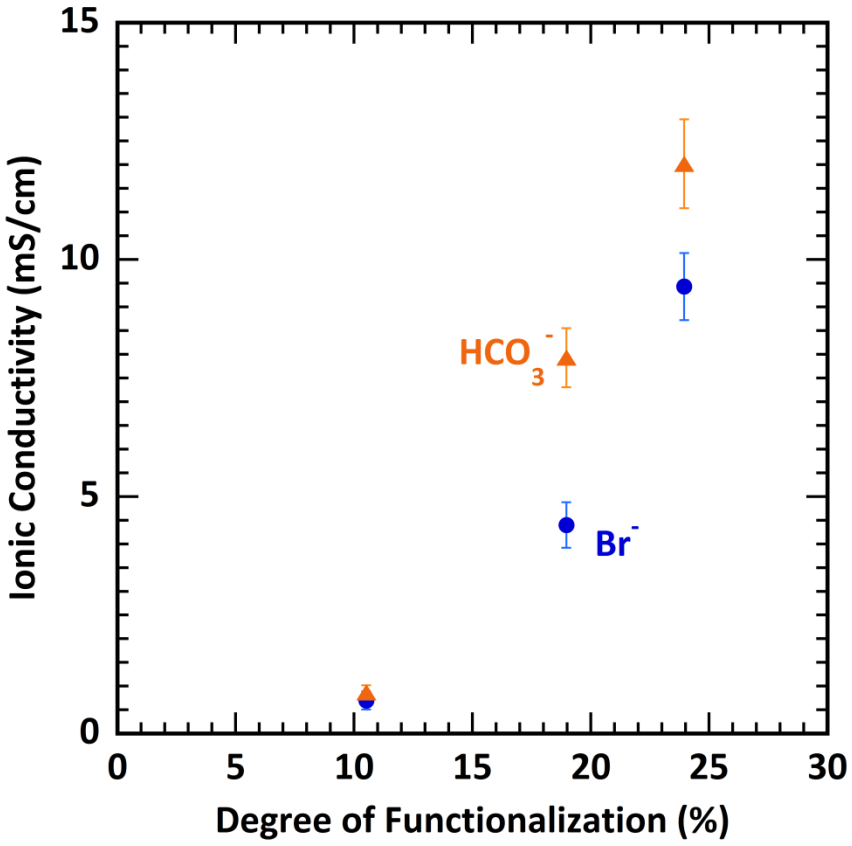

Figure 5. Ionic conductivity as a function of degree of functionalization, χ, for ImPPO-χ materials in Br^- (blue circles) and HCO_3^- (orange triangles) forms.

According to the Nernst-Einstein equation (Eqn 6), membrane conductivity is a function of the concentration of mobile ions in the membrane and the diffusivity of these ions, as follows:[60]

$$\kappa = \frac{F^2}{RT}\sum C_i D_i \qquad \text{Eqn. 6}$$

where F is Faraday's constant, R is the ideal gas constant, T is the absolute temperature, C_i is the concentration of ionic species i, and D_i is the diffusion coefficient of ionic species i. In the

context of the methods used herein, the mobile ion available to contribute to conductivity is the counterion, whose concentration, based on electroneutrality, is proportional to the fixed charge density of the membrane. Given that smaller ions typically have higher diffusivities than relatively larger ions, it is expected that a membrane with a smaller counterion would exhibit a higher ionic conductivity than a membrane with a larger counterion, as has been reported elsewhere.[64,69] However, in this family of ImPPO-χ materials, membranes with the larger bicarbonate counterion exhibited higher conductivities than membranes with the smaller bromide counterion.[70,71] Considering Eqn. 3 (fixed charge concentration) and Eqn. 5 (solute diffusion coefficient), it is clear that ionic conductivity also depends on water volume fraction. As the water volume fraction increases (due to an increased degree of functionalization or a change in the counterion species) the fixed charge concentration decreases and the solute diffusion coefficient increases. Therefore, the fixed charge (and mobile counterion) concentration and the solute diffusion coefficient play opposite roles in determining the effect of increasing water volume fraction on ion conductivity.[35] Within the family of ImPPO-χ materials prepared herein, conductivity depended exponentially on inverse water volume fraction (Figure 6), in agreement with the free volume theory and other studies of AEMs.[22,23,61,62] These results suggest that changes in the structure of the membrane (specifically the free volume available for solute transport) impacted the conductivity of the membrane to a greater degree than changes in ion concentration or size. The bicarbonate and bromide forms of the Selemion AMV membrane exhibited ionic conductivities similar to that expected for ImPPO-χ membranes of the same water volume fraction, as demonstrated in Figure 6 by their proximity to the regression of the ImPPO-χ results.

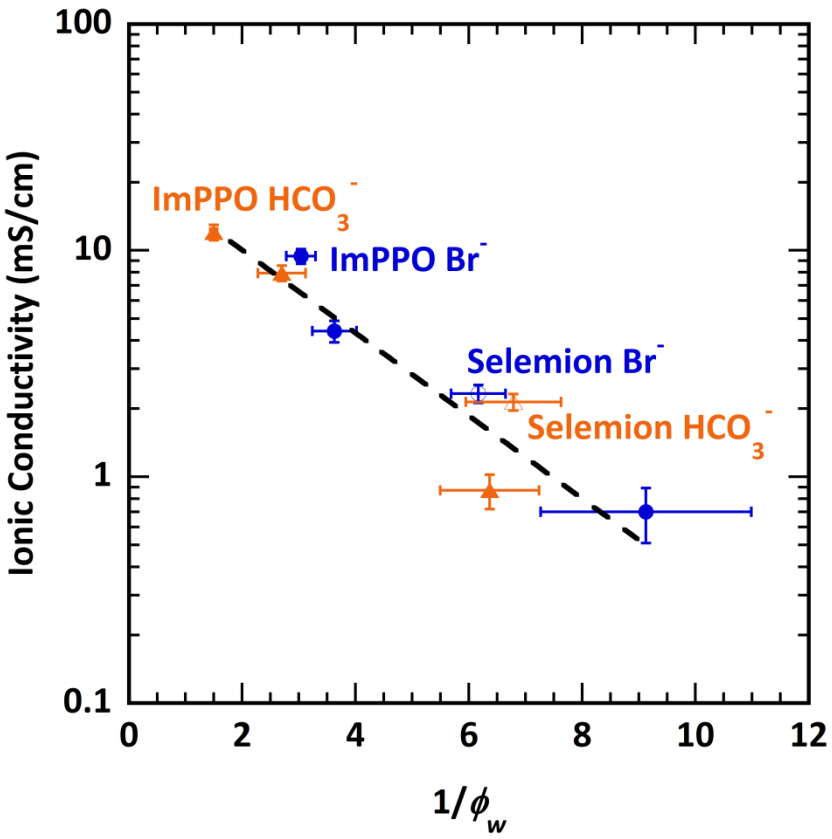

Figure 6. Ionic conductivity as a function of inverse water volume fraction for ImPPO-χ (filled symbols) and Selemion AMV (empty symbols) membranes in Br^- (blue circles) and HCO_3^- (orange triangles) forms. The line is a regression on the ImPPO-χ membrane data.

No significant correlation was observed between conductivity and fixed charge density (Figure S7 in the Supplemental Information), which is not surprising given that previous studies have documented both an increase and a decrease in conductivity with increasing fixed charge density.[23,35] These conflicting results could be explained by competing consequences of water uptake, as discussed above in the context of the Nernst-Einstein equation. In the case of the family of ImPPO-χ materials presented herein, the absence of a trend between ionic conductivity

and fixed charge density suggests that the increase in free volume counterbalances the effect of decreased mobile charge concentration on ionic conductivity.

3.3 Consideration of the ImPPO-χ material platform for artificial photosynthesis devices

As mentioned in the introduction, the most desirable AEMs for artificial photosynthesis have both a high conductivity of charge carriers and a low permeability to the liquid products.[6] Within the family of ImPPO-χ materials, water volume fraction significantly impacted both the ionic conductivity and ethanol permeability, where both increased with increasing water volume fraction. Consequently, an increase in ionic conductivity was correlated with an increase in ethanol permeability (Figure 7). A trade-off between ionic conductivity and CO_2R product permeability can be identified in regard to device operation: beneficial increases in ionic conductivity may be offset by a simultaneous detrimental increase in CO_2R product permeability. While it is difficult to quantify the selectivity of the membrane (*i.e.*, transport of bicarbonate over ethanol) given the difference of driving forces between these two solutes in this context, future work may gain value from measuring the simultaneous transport of both solute species in these materials under applied potentials and ethanol concentration gradients typically encountered in photosynthesis devices. In light of the widespread use of Selemion AMV in studies on artificial photosynthesis devices, membranes of similar conductivities would also be expected to support artificial photosynthesis device performance.[6,7,15,32,72] As the conductivity of Selemion AMV is similar to those of ImPPO-χ materials with low degrees of functionalization (Figure 7), future development of membranes for artificial photosynthesis may focus on materials with relatively low conductivity in order to reduce product crossover.

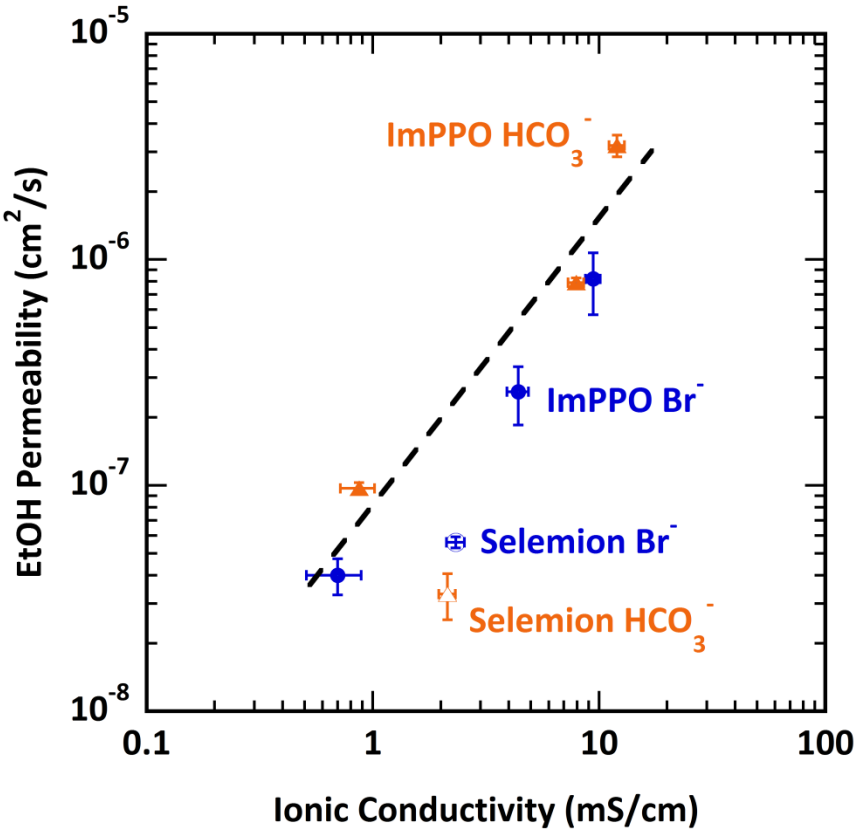

Figure 7. The tradeoff between ethanol permeability and ionic conductivity for ImPPO-χ (filled symbols) and Selemion AMV (empty symbols) membranes in Br^- (blue circles) and HCO_3^- (orange triangles) forms. The line is included to guide the eye over ImPPO-χ data.

While this work demonstrates that water impacts the transport of liquid products and charge carriers through the membrane, the transport of water itself through the membrane may become an important parameter in artificial photosynthesis devices, specifically in those based on membrane-electrode assemblies (MEAs). For example, in MEAs in which the cathode feed is humidified gas and the anode contacts aqueous electrolyte, water diffuses from the anode across the membrane to the cathode. If the transport of water across the membrane is too great, liquid water can flood the cathode, inhibiting CO_2R.[13] Alternatively, in MEAs in which both anode and

cathode are fed humidified gas, the membrane may dehydrate, leading to a loss of ionic conductivity and deterioration of cell performance.[13] Considering such situations, the membrane water uptake, which correlates with water permeability *via* the water volume fraction, may play a critical role in managing water availability inside artificial photosynthesis devices.[13,63]

Conclusions

A family of ImPPO-χ polymers were synthesized and subsequently fabricated into membranes to enable a structure-transport study relevant to artificial photosynthesis. The membrane chemical structure was varied by changing the degree of imidazolium functionalization. Increased degree of functionalization induced an increase in water uptake, suggesting a change in the membrane's physical structure (*i.e.*, an increase in the free volume) as the water volume fraction changed. An increase in the water volume fraction was correlated to an increase in both the ionic conductivity and the ethanol permeability according to the free volume theory. Consequently, ethanol permeability increased with ionic conductivity, leading to a trade-off in the transport parameters desirable for artificial photosynthesis (*i.e.*, high ionic conductivity and low CO_2R product permeability). In light of the structure-property relationships discussed herein, future studies of the ImPPO-χ membrane platform in test-bed artificial photosynthesis devices may enable a valuable correlation between the *ex situ* properties studied herein and device performance. More studies should also be performed to understand the difference in transport properties between Selemion and the ImPPO-χ materials.

Conflict of Interest Disclosure

There are no conflicts of interest to declare.

Supporting information: example NMR spectra; calculation of the degree of functionalization and ion exchange capacity; example EDS spectra; calculation of ethanol permeability; example impedance spectrum and calculation of conductivity; graphical representation of the impact of fixed change concentration on conductivity and ethanol permeability

Acknowledgements

This material is based upon work performed at the Joint Center for Artificial Photosynthesis, a DOE Energy Innovation Hub, supported through the Office of Science of the U.S. Department of Energy under Award Number DE-SC00493.

References

(1) Michl, J. Photochemical CO 2 Reduction: Towards an Artificial Leaf? *Nat. Chem.* **2011**, *3* (4), 268–269. https://doi.org/10.1038/nchem.1021.

(2) Kim, D.; Sakimoto, K. K.; Hong, D.; Yang, P. Artificial Photosynthesis for Sustainable Fuel and Chemical Production. *Angew. Chemie - Int. Ed.* **2015**, *54* (11), 3259–3266. https://doi.org/10.1002/anie.201409116.

(3) Ganesh, I. Conversion of Carbon Dioxide into Methanol - A Potential Liquid Fuel: Fundamental Challenges and Opportunities (a Review). *Renew. Sustain. Energy Rev.* **2014**, *31*, 221–257. https://doi.org/10.1016/j.rser.2013.11.045.

(4) Kumar, B.; Llorente, M.; Froehlich, J.; Dang, T.; Sathrum, A.; Kubiak, C. P. Photochemical and Photoelectrochemical Reduction of CO 2 . *Annu. Rev. Phys. Chem.* **2012**, *63* (1), 541–569. https://doi.org/10.1146/annurev-physchem-032511-143759.

(5) Singh, M. R.; Bell, A. T. Design of an Artificial Photosynthetic System for Production of Alcohols in High Concentration from CO2. *Energy Environ. Sci.* **2016**, *9* (1), 193–199. https://doi.org/10.1039/c5ee02783g.

(6) Singh, M. R.; Clark, E. L.; Bell, A. T. Effects of Electrolyte, Catalyst, and Membrane Composition and Operating Conditions on the Performance of Solar-Driven Electrochemical Reduction of Carbon Dioxide. *Phys. Chem. Chem. Phys.* **2015**, *17* (29), 18924–18936. https://doi.org/10.1039/c5cp03283k.

(7) Patru, A.; Binninger, T.; Pribyl, B.; Schmidt, T. J. Design Principles of Bipolar Electrochemical Co-Electrolysis Cells for Efficient Reduction of Carbon Dioxide from Gas Phase at Low Temperature. *J. Electrochem. Soc.* **2019**, *166* (2), 34–43. https://doi.org/10.1149/2.1221816jes.

(8) Kutz, R. B.; Chen, Q.; Yang, H.; Sajjad, S. D.; Liu, Z.; Masel, I. R. Sustainion Imidazolium-Functionalized Polymers for Carbon Dioxide Electrolysis. *Energy Technol.* **2017**, *5*, 929–936. https://doi.org/10.1002/ente.201600636.

(9) Nitopi, S.; Bertheussen, E.; Scott, S. B.; Liu, X.; Engstfeld, A. K.; Horch, S.; Seger, B.; Stephens, I. E. L.; Chan, K.; Hahn, C.; et al. Progress and Perspectives of Electrochemical CO2 Reduction on Copper in Aqueous Electrolyte. *Chem. Rev.* **2019**, *119* (12), 7610–7672. https://doi.org/10.1021/acs.chemrev.8b00705.

(10) Wang, L.; Nitopi, S. A.; Bertheussen, E.; Orazov, M.; Morales-Guio, C. G.; Liu, X.; Higgins, D. C.; Chan, K.; Nørskov, J. K.; Hahn, C.; et al. Electrochemical Carbon Monoxide Reduction on Polycrystalline Copper: Effects of Potential, Pressure, and PH on Selectivity toward Multicarbon and Oxygenated Products. *ACS Catal.* **2018**, *8* (8), 7445–7454. https://doi.org/10.1021/acscatal.8b01200.

(11) Xiao, H.; Cheng, T.; Goddard III, W. A.; Sundararaman, R. Mechanistic Explanation of the PH Dependence and Onset Potentials for Hydrocarbon Products from Electrochemical Reduction of CO on Cu (111). *J. Am. Chem. Soc.* **2016**, *138*, 486–486. https://doi.org/10.1021/jacs.5b11390.

(12) Resasco, J.; Chen, L. D.; Clark, E.; Tsai, C.; Hahn, C.; Jaramillo, T. F.; Chan, K.; Bell, A. T. Promoter Effects of Alkali Metal Cations on the Electrochemical Reduction of Carbon Dioxide. *J. Am. Chem. Soc.* **2017**, *139* (32), 11277–11287. https://doi.org/10.1021/jacs.7b06765.

(13) Weng, L. C.; Bell, A. T.; Weber, A. Z. Towards Membrane-Electrode Assembly Systems for CO2 Reduction: A Modeling Study. *Energy Environ. Sci.* **2019**, *12* (6), 1950–1968. https://doi.org/10.1039/c9ee00909d.

(14) Higgins, D.; Hahn, C.; Xiang, C.; Jaramillo, T. F.; Weber, A. Z. Gas-Diffusion Electrodes for Carbon Dioxide Reduction: A New Paradigm. *ACS Energy Lett.* **2019**, *4* (1), 317–324. https://doi.org/10.1021/acsenergylett.8b02035.

(15) Hori, Y.; Ito, H.; Okano, K.; Nagasu, K.; Sato, S. Silver-Coated Ion Exchange Membrane Electrode Applied to Electrochemical Reduction of Carbon Dioxide. *Electrochim. Acta* **2003**, *48* (18), 2651–2657. https://doi.org/10.1016/S0013-4686(03)00311-6.

(16) Jin, J.; Walczak, K.; Singh, M. R.; Karp, C.; Lewis, N. S.; Xiang, C. An Experimental and Modeling/Simulation-Based Evaluation of the Efficiency and Operational Performance Characteristics of an Integrated, Membrane-Free, Neutral PH Solar-Driven Water-Splitting System. *Energy Environ. Sci.* **2014**, *7* (10), 3371–3380. https://doi.org/10.1039/c4ee01824a.

(17) Kuhl, K. P.; Cave, E. R.; Abram, D. N.; Jaramillo, T. F. New Insights into the

Electrochemical Reduction of Carbon Dioxide on Metallic Copper Surfaces. *Energy Environ. Sci.* **2012**, *5* (5), 7050–7059. https://doi.org/10.1039/c2ee21234j.

(18) Ong, B. C.; Kamarudin, S. K.; Basri, S. Direct Liquid Fuel Cells : A Review. *Int. J. Hydrogen Energy* **2017**, *42*, 10142–10157. https://doi.org/10.1016/j.ijhydene.2017.01.117.

(19) Merle, G.; Wessling, M.; Nijmeijer, K. Anion Exchange Membranes for Alkaline Fuel Cells: A Review. *J. Memb. Sci.* **2011**, *377* (1–2), 1–35. https://doi.org/10.1016/j.memsci.2011.04.043.

(20) Pan, Z. F.; An, L.; Zhao, T. S.; Tang, Z. K. Advances and Challenges in Alkaline Anion Exchange Membrane Fuel Cells. *Prog. Energy Combust. Sci.* **2018**, *66*, 141–175. https://doi.org/10.1016/j.pecs.2018.01.001.

(21) Yang, H.; Kaczur, J. J.; Sajjad, S. D.; Masel, R. I. Electrochemical Conversion of CO2 to Formic Acid Utilizing Sustainion™ Membranes. *J. CO2 Util.* **2017**, *20* (April), 208–217. https://doi.org/10.1016/j.jcou.2017.04.011.

(22) Carter, B. M.; Keller, L.; Wessling, M.; Miller, D. J. Preparation and Characterization of Crosslinked Poly(Vinylimidazolium) Anion Exchange Membranes for Artificial Photosynthesis. *J. Mater. Chem. A* **2019**. https://doi.org/10.1039/c9ta00498j.

(23) Geise, G. M.; Hickner, M. A.; Logan, B. E. Ionic Resistance and Permselectivity Tradeoffs in Anion Exchange Membranes. *Appl. Mater. Interfaces* **2013**, *5*, 10294–10301.

(24) Park, H. B.; Kamcev, J.; Robeson, L. M.; Elimelech, M.; Freeman, B. D. Maximizing the Right Stuff: The Trade-off between Membrane Permeability and Selectivity. *Science* **2017**, *356* (6343). https://doi.org/10.1126/science.aab0530.

(25) Geise, G. M.; Park, H. B.; Sagle, A. C.; Freeman, B. D.; McGrath, J. E. Water Permeability and Water/Salt Selectivity Tradeoff in Polymers for Desalination. *J. Memb.*

Sci. **2011**, *369* (1–2), 130–138. https://doi.org/10.1016/j.memsci.2010.11.054.

(26) Zhang, H.; Shen, P. K. Advances in the High Performance Polymer Electrolyte Membranes for Fuel Cells. *Chem. Soc. Rev.* **2012**, *41* (6), 2382–2394. https://doi.org/10.1039/c2cs15269j.

(27) Gottesfeld, S.; Dekel, D. R.; Page, M.; Bae, C.; Yan, Y.; Zelenay, P.; Kim, Y. S. Anion Exchange Membrane Fuel Cells: Current Status and Remaining Challenges. *J. Power Sources* **2018**, *375*, 170–184. https://doi.org/10.1016/j.jpowsour.2017.08.010.

(28) Kamcev, J.; Freeman, B. D. Charged Polymer Membranes for Environmental/Energy Applications. *Annu. Rev. Chem. Biomol. Eng.* **2016**, *7* (1), 111–133. https://doi.org/10.1146/annurev-chembioeng-080615-033533.

(29) Luo, T.; Abdu, S.; Wessling, M. Selectivity of Ion Exchange Membranes: A Review. *J. Memb. Sci.* **2018**, *555* (December 2017), 429–454. https://doi.org/10.1016/j.memsci.2018.03.051.

(30) Le, X. T.; Bui, T. H.; Viel, P.; Berthelot, T.; Palacin, S. On the Structure-Properties Relationship of the AMV Anion Exchange Membrane. *J. Memb. Sci.* **2009**, *340* (1–2), 133–140. https://doi.org/10.1016/j.memsci.2009.05.025.

(31) Kingsbury, R. S.; Zhu, S.; Flotron, S.; Coronell, O. Microstructure Determines Water and Salt Permeation in Commercial Ion-Exchange Membranes. *ACS Appl. Mater. Interfaces* **2018**, *10* (46), 39745–39756. https://doi.org/10.1021/acsami.8b14494.

(32) Merino-Garcia, I.; Alvarez-Guerra, E.; Albo, J.; Irabien, A. Electrochemical Membrane Reactors for the Utilisation of Carbon Dioxide. *Chem. Eng. J.* **2016**, *305*, 104–120. https://doi.org/10.1016/j.cej.2016.05.032.

(33) Yan, N.; Paul, D. R.; Freeman, B. D. Water and Ion Sorption in a Series of Cross-Linked

AMPS/PEGDA Hydrogel Membranes. *Polymer (Guildf).* **2018**, *146*, 196–208. https://doi.org/10.1016/j.polymer.2018.05.021.

(34) Zhu, S.; Kingsbury, R. S.; Call, D. F.; Coronell, O. Impact of Solution Composition on the Resistance of Ion Exchange Membranes. *J. Memb. Sci.* **2018**, *554* (November 2017), 39–47. https://doi.org/10.1016/j.memsci.2018.02.050.

(35) Fan, H.; Yip, N. Y. Elucidating Conductivity-Permselectivity Tradeoffs in Electrodialysis and Reverse Electrodialysis by Structure-Property Analysis of Ion-Exchange Membranes. *J. Memb. Sci.* **2019**, *573* (October 2018), 668–681. https://doi.org/10.1016/j.memsci.2018.11.045.

(36) Carter, B. M.; Dobyns, B. M.; Beckingham, B. S.; Miller, D. J. Multicomponent Transport of Alcohols in an Anion Exchange Membrane Measured by In-Situ ATR FTIR Spectroscopy. *Polym. (United Kingdom)* **2017**, *123*, 144–152. https://doi.org/10.1016/j.polymer.2017.06.070.

(37) Galizia, M.; Paul, D. R.; Freeman, B. D. Liquid Methanol Sorption, Diffusion and Permeation in Charged and Uncharged Polymers. *Polymer (Guildf).* **2016**, *102*, 281–291. https://doi.org/10.1016/j.polymer.2016.09.010.

(38) Gu, S.; Skovgard, J.; Yan, Y. S. Engineering the van Der Waals Interaction in Cross-Linking-Free Hydroxide Exchange Membranes for Low Swelling and High Conductivity. *ChemSusChem* **2012**, *5* (5), 843–848. https://doi.org/10.1002/cssc.201200057.

(39) Mohanty, A. D.; Tignor, S. E.; Krause, J. A.; Choe, Y.-K.; Bae, C. Systematic Alkaline Stability Study of Polymer Backbones for Anion Exchange Membrane Applications. *Macromolecules* **2016**, *49* (9), 3361–3372. https://doi.org/10.1021/acs.macromol.5b02550.

(40) Arges, C. G.; Wang, L.; Parrondo, J.; Ramani, V. Best Practices for Investigating Anion Exchange Membrane Suitability for Alkaline Electrochemical Devices: Case Study Using Quaternary Ammonium Poly(2,6-Dimethyl 1,4-Phenylene)Oxide Anion Exchange Membranes. *J. Electrochem. Soc.* **2013**, *160* (11), F1258–F1274. https://doi.org/10.1149/2.049311jes.

(41) Zhao, L.; Chang, P. C.-Y.; Ho, W. S. W. High-Flux Reverse Osmosis Membranes Incorporated with Hydrophilic Additives for Brackish Water Desalination. *Desalination* **2013**, *308*, 225–232. https://doi.org/10.1016/j.desal.2012.07.020.

(42) Ran, J.; Wu, L.; Varcoe, J. R.; Ong, A. L.; Poynton, S. D.; Xu, T. Development of Imidazolium-Type Alkaline Anion Exchange Membranes for Fuel Cell Application. *J. Memb. Sci.* **2012**, *415–416*, 242–249. https://doi.org/10.1016/j.memsci.2012.05.006.

(43) Hossain, M. M.; Hou, J.; Wu, L.; Ge, Q.; Liang, X.; Mondal, A. N.; Xu, T. Anion Exchange Membranes with Clusters of Alkyl Ammonium Group for Mitigating Water Swelling but Not Ionic Conductivity. *J. Memb. Sci.* **2018**, *550*, 101–109. https://doi.org/10.1016/j.memsci.2017.12.062.

(44) Tongwen, X.; Weihua, Y. Fundamental Studies of a New Series of Anion Exchange Membranes: Membrane Preparation and Characterization. *J. Memb. Sci.* **2001**, *190* (2), 159–166.

(45) Pan, J.; Han, J.; Zhu, L.; Hickner, M. A. Cationic Side-Chain Attachment to Poly(Phenylene Oxide) Backbones for Chemically Stable and Conductive Anion Exchange Membranes. *Chem. Mater.* **2017**, *29* (12), 5321–5330. https://doi.org/10.1021/acs.chemmater.7b01494.

(46) Lin, B.; Qiu, L.; Lu, J.; Yan, F. Cross-Linked Alkaline Ionic Liquid-Based Polymer

Electrolytes for Alkaline Fuel Cell Applications. *Chem. Mater.* **2010**, *22* (24), 6718–6725. https://doi.org/10.1021/cm102957g.

(47) Ye, Y.; Elabd, Y. A. Relative Chemical Stability of Imidazolium-Based Alkaline Anion Exchange Polymerized Ionic Liquids. *Macromolecules* **2011**, *44* (21), 8494–8503. https://doi.org/10.1021/ma201864u.

(48) Li, N.; Leng, Y.; Hickner, M. A.; Wang, C. Highly Stable, Anion Conductive, Comb-Shaped Copolymers for Alkaline Fuel Cells. *J. Am. Chem. Soc.* **2013**, *135*, 10124–10133.

(49) Zhang, K.; McDonald, M. B.; Genina, I. E. A.; Hammond, P. T. A Highly Conductive and Mechanically Robust OH- Conducting Membrane for Alkaline Water Electrolysis. *Chem. Mater.* **2018**, *30* (18), 6420–6430. https://doi.org/10.1021/acs.chemmater.8b02709.

(50) Dang, H.-S.; Jannasch, P. A Comparative Study of Anion-Exchange Membranes Tethered with Different Hetero-Cycloaliphatic Quaternary Ammonium Hydroxides. *J. Mater. Chem. A* **2017**, 21965–21978. https://doi.org/10.1039/C7TA06029G.

(51) Gustafsson, J. P. Visual MINTEQ, Ver. 3.1. KTH, SEED: Stockholm, Sweden 2019.

(52) Harris, D. C. *Quantitative Chemical Analysis*, 6th Ed.; W. H. Freeman and Company: New York, 2003.

(53) Geise, G. M.; Paul, D. R.; Freeman, B. D. Fundamental Water and Salt Transport Properties of Polymeric Materials. *Prog. Polym. Sci.* **2014**, *39* (1), 1–24. https://doi.org/10.1016/j.progpolymsci.2013.07.001.

(54) Beckingham, B. S.; Lynd, N. A.; Miller, D. J. Monitoring Multicomponent Transport Using in Situ ATR FTIR Spectroscopy. *J. Memb. Sci.* **2018**, *550* (December 2017), 348–356. https://doi.org/10.1016/j.memsci.2017.12.072.

(55) Fontananova, E. Impedance Spectroscopy, Membrane Characterization By. In

Encyclopedia of Membranes; Drioli, E., Giorno, L., Eds.; Springer, Berlin, Heidelberg, 2016. https://doi.org/https://doi.org/10.1007/978-3-662-44324-8.

(56) Liu, Y.; Wang, J.; Yang, Y.; Brenner, T. M.; Seifert, S.; Yan, Y.; Liberatore, M. W.; Herring, A. M. Anion Transport in a Chemically Stable, Sterically Bulky α-C Modified Imidazolium Functionalized Anion Exchange Membrane. *J. Phys. Chem. C* **2014**, *118* (28), 15136–15145. https://doi.org/10.1021/jp5027674.

(57) Gopi, K. H.; Peera, S. G.; Bhat, S. D.; Sridhar, P.; Pitchumani, S. Preparation and Characterization of Quaternary Ammonium Functionalized Poly(2,6-Dimethyl-1,4-Phenylene Oxide) as Anion Exchange Membrane for Alkaline Polymer Electrolyte Fuel Cells. *Int. J. Hydrogen Energy* **2014**, *39* (6), 2659–2668. https://doi.org/10.1016/j.ijhydene.2013.12.009.

(58) Parrondo, J.; Jung, M. J.; Wang, Z.; Arges, C. G.; Ramani, V. Synthesis and Alkaline Stability of Solubilized Anion Exchange Membrane Binders Based on Poly(Phenylene Oxide) Functionalized with Quaternary Ammonium Groups via a Hexyl Spacer. *J. Electrochem. Soc.* **2015**, *162* (10), F1236–F1242. https://doi.org/10.1149/2.0891510jes.

(59) Yang, J.; Liu, C.; Hao, Y.; He, X.; He, R. Preparation and Investigation of Various Imidazolium-Functionalized Poly(2,6-Dimethyl-1,4-Phenylene Oxide) Anion Exchange Membranes. *Electrochim. Acta* **2016**, *207*, 112–119. https://doi.org/10.1016/j.electacta.2016.04.176.

(60) Kamcev, J.; Sujanani, R.; Jang, E.; Yan, N.; Moe, N.; Paul, D. R.; Freeman, B. D. Salt Concentration Dependence of Ionic Conductivity in Ion Exchange Membranes. *J. Memb. Sci.* **2018**, *547*, 123–133. https://doi.org/10.1016/j.memsci.2017.10.024.

(61) Yasuda, H.; Lamaze, C. E.; Ikenberry, L. D. Permeability of Solutes through Hydrated

Polymer Membranes Part I. Diffusion of Sodium Chloride. *Die Makromol. Chemie* **1968**, *118*, 19–35.

(62) Yasuda, H.; Ikenberry, L. D.; Lamaze, C. E. Permeability of Solutes through Hydrated Polymer Membranes. Part II. Permeability of Water Soluble Organic Solutes. *Die Makromol. Chemie* **1968**, *125* (3062), 108–118.

(63) Xie, W.; Ju, H.; Geise, G. M.; Freeman, B. D.; Mardel, J. I.; Hill, A. J.; McGrath, J. E. Effect of Free Volume on Water and Salt Transport Properties in Directly Copolymerized Disulfonated Poly(Arylene Ether Sulfone) Random Copolymers. *Macromolecules* **2011**, *44* (11), 4428–4438. https://doi.org/10.1021/ma102745s.

(64) Amel, A.; Gavish, N.; Zhu, L.; Dekel, D. R.; Hickner, M. A.; Ein-Eli, Y. Bicarbonate and Chloride Anion Transport in Anion Exchange Membranes. *J. Memb. Sci.* **2016**, *514*, 125–134. https://doi.org/10.1016/j.memsci.2016.04.027.

(65) Rustad, J. R.; Nelmes, S. L.; Jackson, V. E.; Dixon, D. A. Quantum-Chemical Calculations of Carbon-Isotope Fractionation in CO 2(g), Aqueous Carbonate Species, and Carbonate Minerals. *J. Phys. Chem. A* **2008**, *112* (3), 542–555. https://doi.org/10.1021/jp076103m.

(66) Raugei, S.; Klein, M. L. Dynamics of Water Molecules in the Br- Solvation Shell: An Ab Initio Molecular Dynamics Study. *J. Am. Chem. Soc.* **2001**, *123* (38), 9484–9485. https://doi.org/10.1021/ja011030k.

(67) Wijmans, J. G.; Baker, R. W. The Solution-Diffusion Model: A Review. *J. Memb. Sci.* **1995**, *107*, 1–21. https://doi.org/10.1016/0376-7388(95)00102-I.

(68) Masaro, L.; Zhu, X. X. *Physical Models of Diffusion for Polymer Solutions, Gels and Solids*; 1999; Vol. 24. https://doi.org/10.1016/S0079-6700(99)00016-7.

(69) Le, X. T. Concentration Polarization and Conductance of Cation Exchange Membranes in Sulfuric Acid and Alkaline Sulfate Media. *J. Memb. Sci.* **2012**, *397–398*, 66–79. https://doi.org/10.1016/j.memsci.2012.01.011.

(70) Nightingale, E. R. Phenomenological Theory of Ion Solvation. Effective Radii of Hydrated Ions. *J. Phys. Chem.* **1959**, *63* (9), 1381–1387. https://doi.org/10.1021/j150579a011.

(71) Kiss, A. M.; Myles, T. D.; Grew, K. N.; Peracchio, A. A.; Nelson, G. J.; Chiu, W. K. S. Carbonate and Bicarbonate Ion Transport in Alkaline Anion Exchange Membranes. *J. Electrochem. Soc.* **2013**, *160* (9), F994–F999.

(72) Komatsu, S.; Tanaka, M.; Okumura, A.; Kungi, A. Preparation of Cu-Solid Polymer Electrolyte Composite Electrodes and Application to Gas-Phase Electrochemical Reduction of CO2. *Electrochim. Acta* **1995**, *40* (6), 745–753. https://doi.org/10.1016/0013-4686(94)00325-U.